BULLETIN OF THE POLISH ACADEMY OF SCIENCES
TECHNICAL SCIENCES
DOI: 10.24425/bpasts.2025.153836

Investigation of the Temperature Impact on the Operation of a Nonlinear Electromagnetic Vibration Energy Harvester

Marcin KULIK[1]*, Rafał GABOR[1]

[1] Opole University of Technology, Faculty of Electrical Engineering, Automatic Control and Informatics, Opole

Abstract. This paper presents a detailed study on the impact of temperature on the performance of a nonlinear electromagnetic vibration energy harvester, which is applied in autonomous power systems. The variability of material properties under the influence of temperature, such as stiffness, damping, and magnetic induction, significantly affects the operational characteristics of the device. A mathematical model accounting for these factors, including linear and quadratic temperature coefficients, optimized using a genetic algorithm, is presented in the article. The simulation results were compared with experimental data, showing good agreement, particularly in the range of frequency bandwidth and output voltage. It was demonstrated that higher temperatures lead to a reduction in mechanical and magnetic stiffness, resulting in decreased energy conversion efficiency.

Key words: energy harvesting; nonlinear electromagnetic energy harvester; temperature coefficients; frequency response; dynamic analysis

1. INTRODUCTION

In recent years, nonlinear vibration energy harvesters have gained popularity as potential solutions in the field of sustainable energy and autonomous power systems [1–3]. They are particularly interesting for powering small devices, sensors, and in the growing "Internet of Things" (IoT) technology [1,4–9]. The ability to harvest energy from the environment can significantly extend the operating time of devices without the need for charging, battery replacement, or may entirely eliminate the necessity of using wired connections [10,11]. These harvesters, utilizing nonlinear mechanisms to optimize energy collection from various, often irregular, vibrations of variable frequency, are becoming crucial in the development of modern technologies, providing a wide frequency range for effective energy harvesting [1,12,13].

The small size of mini-generators requires a highly restrictive design approach, often fully utilizing the material properties of the components used. In the design process of such energy harvesters, optimization algorithms are employed to obtain information on the material, geometric, and load parameters for the given input data [13]. However, it should be noted that the actual construction of the device is often subject to uncertainties compared to the modeled geometric and material parameters [14,15].

In light of the growing popularity and applications of vibration energy harvesters, a critical aspect of their efficiency is operational stability under various environmental conditions [16]. One of the fundamental factors affecting the performance of these devices is the ambient temperature [17]. Temperature fluctuations can significantly influence the properties of the materials used in the harvester's construction, causing changes in the stiffness or damping of key components. These changes directly affect the vibration dynamics and, thus, the efficiency and performance of the harvester [12].

There are publications [17,18] in which the authors studied the effect of temperature on the magnetic and mechanical properties of various harvesters; however, the nonlinear characteristics of the presented family of energy harvesters make understanding the impact of temperature on their performance a complex but necessary task for optimizing their design and operation.

The aim of this paper is to experimentally investigate the impact of temperature on the power and output voltage of nonlinear vibration energy harvesters. The second aspect of the work is the identification of temperature coefficients, which, when introduced into the mathematical model, will allow the simulation of the operation of nonlinear energy harvesting systems under different temperature conditions.

2. CONSIDERED NONLINEAR ELECTROMAGNETIC VIBRATION ENERGY HARVESTER

The energy harvester considered in this study is an electromagnetic vibration energy mini-generator utilizing the phenomenon of mechanical resonance (Fig. 1a). The vibrating structural element is a flat beam made of a composite material reinforced with fiberglass, with one end attached to the housing,

*e-mail: m.kulik@po.edu.pl

while the other end holds yokes with permanent magnets. The generator system is mounted directly on the vibration source, causing the permanent magnets in the yokes to move relative to stationary coils, which are connected in parallel and placed on the outer sides of the yokes. The movement of the magnets generates a varying magnetic flux in the coils, leading to the induction of an electric voltage. The phenomenon of nonlinear parametric resonance, which allows for a wide operational frequency band, occurs due to the presence of internal magnetic forces caused by the interaction of the moving permanent magnets in the yokes with additional permanent magnets [19, 20]. The stationary permanent magnets are placed in a vertical support located between the yokes.

The mathematical model of the nonlinear electromagnetic mini-generator with parameters presented in Fig. 1a can be described by the following equations:

$$m\frac{d^2\zeta(t)}{dt^2} + c(T)\frac{d\zeta(t)}{dt} + \left[k(T) + k_{\mathrm{mag}}(\zeta,T)\right]\zeta(t) = ma_{\mathrm{vib}}(t) - mg - \frac{\partial\lambda(\zeta,T)}{\partial\zeta}i. \quad (1)$$

$$L_{\mathrm{c}}\frac{di(t)}{dt} = \frac{\partial\lambda(\zeta,T)}{\partial\zeta}\frac{d\zeta(t)}{dt} - \left(R_{\mathrm{L}} + R_{\mathrm{c}}(T)\right)i. \quad (2)$$

$$a_{\mathrm{vib}}(t) = a_{\mathrm{rms}}\sqrt{2}sin\,(2\pi ft),. \quad (3)$$

where:

m – mass of the vibrating part, c – damping coefficient, k – stiffness coefficient, k_{mag} – stiffness coefficient due to magnetic force, ζ – displacement of the vibrating part, a_{vib} – external vibrations, a_{rms} – RMS value of vibrations, f – vibration frequency, g – gravitational acceleration, λ – flux linkage with the winding, i – current in the winding, L_c – winding inductance, R_c – winding resistance, R_L – load resistance, t – time, T - temperature. Table 1 summarizes the parameter values appearing in equations (1)-(3). The mathematical model assumes vertical motion of the vibrating mass, which is a reasonable approximation for small displacements typical in this system. While the actual motion may have a slight curvilinear component due to the structure's geometry, its effect on the overall dynamics is negligible for the displacement amplitudes considered. This assumption simplifies the analysis without compromising the accuracy of the results.

TABLE 1. Parameter values used in mathematical model (1)-(3)

Parameters	Values
m (kg)	0.046
c (N·s/m) @ 20°C	0.39
k (N/m) @ 20°C	2213
g (m/s^2)	9.81
L_c (H)	0.0017
R_c (Ω) @ 20°C	5.37

Due to the absence of ferromagnetic materials and assuming linearity of the magnetic circuit, the magnetic force can be determined analytically, where the formulas for the force between two cuboidal magnets arranged in a 3D space were

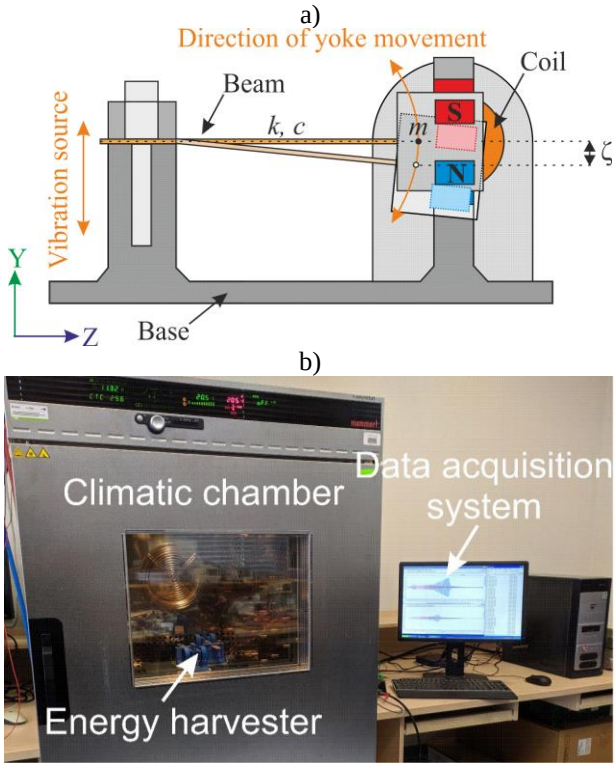

Fig.1. CAD diagram of nonlinear vibration energy harvester using electromagnetic mini-generator (a), Laboratory test-stand with environmental chamber and data acquisition system (b)

derived in [21]. The derivative of the flux linkage with the coil was calculated using Biot-Savart's law, as described in [13]. The nonlinear magnetic stiffness in equation (1) is the magnetic force divided by the displacement

$$k_{\mathrm{mag}}(\zeta,T) = \frac{F_{mag}(\zeta,T)}{\zeta}. \quad (4)$$

Knowing the mechanical stiffness coefficient of the flat beam and the magnetic stiffness behavior for the considered range of yoke displacements, the resonant frequency of the nonlinear electromagnetic energy harvester can be determined using the following formula:

$$f_{\mathrm{res}} = \frac{1}{2\pi}\sqrt{\frac{k(T)+k_{\mathrm{mag}}(\zeta,T)}{m}}. \quad (5)$$

With the proper adjustment of the magnetic stiffness profile, this type of system can achieve frequency characteristics with a broader frequency band compared to a linear system.

The possibility of implementing the harvester in various working environments prompted the authors to conduct a series of studies aimed at identifying the system's behavior under different operating conditions and thermal environments.

3. IDENTIFICATION OF TEMPERATURE COEFFICIENTS

The energy conversion efficiency and reliability of the mini-generator system are influenced by many factors, which are significantly dependent on temperature. The voltage generated by the harvester depends on the remanence induction of the magnets as well as the stiffness and damping of the beam used

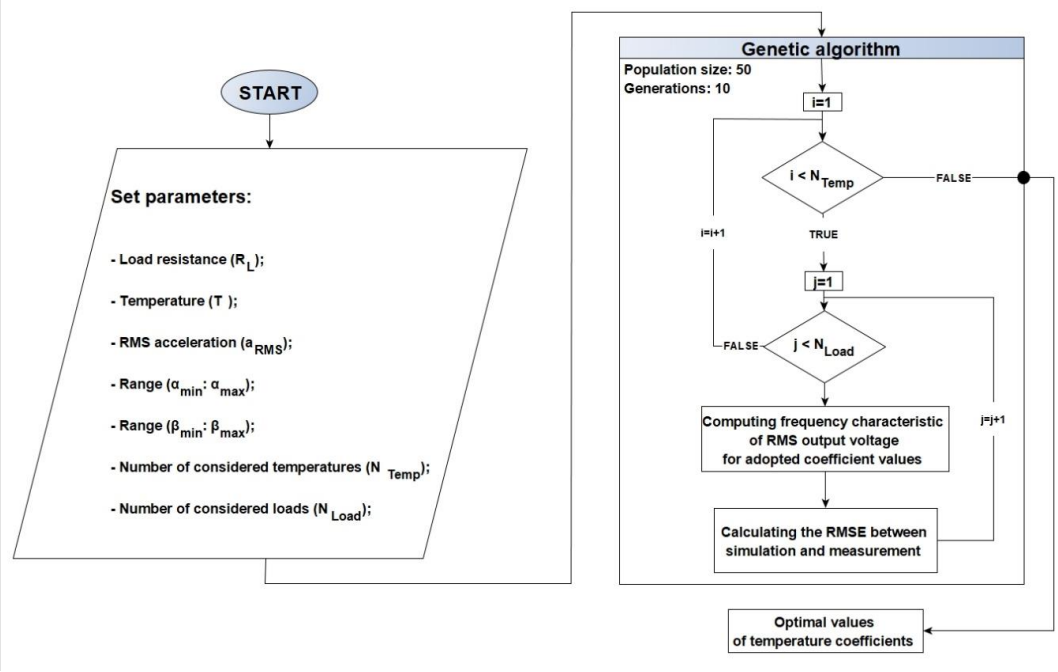

Fig.2. Optimization scheme for the determination of the temperature coefficients (α and β)

in the mini-generator. Knowing that temperature changes affect various material properties and device composites, which in turn reflect on the system's performance and efficiency, the authors introduced temperature coefficients into the mechanical (1) and electrical (2) equations when modeling the harvester. The obtained equations for stiffness (6), damping (7), and remanence induction (8) account for both the linear and quadratic components, where the coefficients α_k, α_c i α_{B_r} represent the linear change in stiffness, damping, and remanence, respectively, while β_k, β_c i β_{B_r} represent the quadratic change of these parameters with respect to temperature

$$k = k_{20°C}(1 + \alpha_k(T - 20°C) + \beta_k(T - 20°C)^2) \quad (6)$$

$$c = c_{20°C}(1 + \alpha_c(T - 20°C) + \beta_c(T - 20°C)^2) \quad (7)$$

$$B_r = B_{r\,20°C}\left(1 + \alpha_{B_r}(T - 20°C) + \beta_{B_r}(T - 20°C)^2\right) \quad (8)$$

In describing the winding resistance in the model, a linear dependence on temperature was assumed, and according to the literature, this coefficient is 0.0393%/°C [22].

To identify the temperature coefficients, frequency response measurements were conducted in a climatic chamber (Fig. 1b). Temperature values were set in the range from 0 to 80°C, load resistance was set at 2, 5, and 10 Ω, and the effective vibration acceleration was set at 10 m/s². Frequency characteristics were obtained for sinusoidal vibrations with an increasing frequency from 15 to 35 Hz and a decreasing frequency from 35 to 15 Hz. After obtaining the measurement results, the range of temperature coefficient values was determined (Table 2). To fit the temperature coefficients of the mathematical model (1)-(8), an optimization process scheme based on a genetic algorithm was created (Fig. 2). For each individual in the population, frequency response characteristics were calculated for each considered temperature and load, and then the root mean squared error of the difference between measured and calculated values was determined. After the final generation in the genetic algorithm, the individual with the minimal error is selected. Calculations were performed in parallel on a computer with a 28-core Intel Xeon E5-2683 v3 2.00 GHz processor and 128 GB of RAM. The temperature coefficients obtained through the optimization process are summarized in Table 3.

TABLE 2. Range of parameters for optimization process

Parameters	Values
Temperature T (°C)	{0, 10, 20, 30, 40, 50, 60, 70, 80}
Load resistance R_L (Ω)	{2, 5, 10}
Acceleration of vibration a_{RMS} (m/s^2)	10
Linear temperature coefficients (%/°C)	$-0.5 \le \alpha_k \le -0.05$
	$0.1 \le \alpha_c \le 0.5$
	$-0.12 \le \alpha_{B_r} \le -0.09$
Quadratic temperature coefficients (%/°C)	$-0.01 \le \beta_k \le 0.01$
	$-0.01 \le \beta_c \le 0.01$
	$-0.01 \le \beta_{B_r} \le 0.01$

TABLE 3. Optimized temperature coefficient

Parameters	Values
Linear temperature coefficients (%/°C)	$\alpha_k = -0.078$
	$\alpha_c = 0.25$
	$\alpha_{B_r} = -0.11$
Quadratic temperature coefficients (%/°C)	$\beta_k = -0.0031$
	$\beta_c = 0.0051$
	$\beta_{B_r} = -0.0009$

Figure 3 presents three sets of frequency response characteristics of the RMS voltage for different ambient temperatures with an acceleration of 10 m/s². The sets of characteristics differ in terms of load resistance. These characteristics were obtained for an increasing vibration frequency from 15 to 35 Hz. As can be seen, the obtained model provides results very close to the measurements. The largest differences can be observed at a temperature of 80°C, but they do not exceed 0.03 V. The maximum value of 0.95 V was obtained for a load of 10 Ω, a frequency of 29.6 Hz, and an ambient temperature of 0°C. For each considered load, a decrease in voltage (approximately 0.1 V for a 10 Ω load) is observed as the temperature increases. The broadest frequency band in which a relatively high voltage is generated occurs at 30°C. A significant narrowing of the band was observed at an ambient temperature of 80°C due to the reduced stiffness of the beam.

Figure 4 shows the simulation and measurement results for a decreasing vibration frequency from 35 to 15 Hz. Due to the nonlinear magnetic force F_{mag}, hysteresis occurs in this system, meaning that the values obtained when decreasing the vibration frequency differ significantly from those obtained when increasing the frequency. The main difference is the bandwidth, which is much smaller in the case of decreasing frequency. The

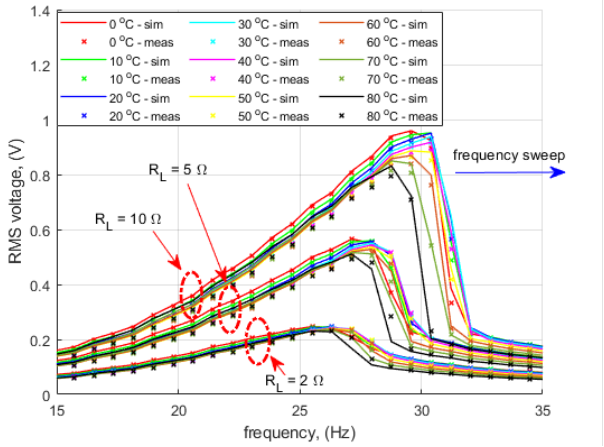

Fig.3. Measured and calculated frequency response characteristics of the RMS voltage for different temperatures and loads at an acceleration of 10 m/s² – vibration frequency increasing from 15 to 35 Hz.

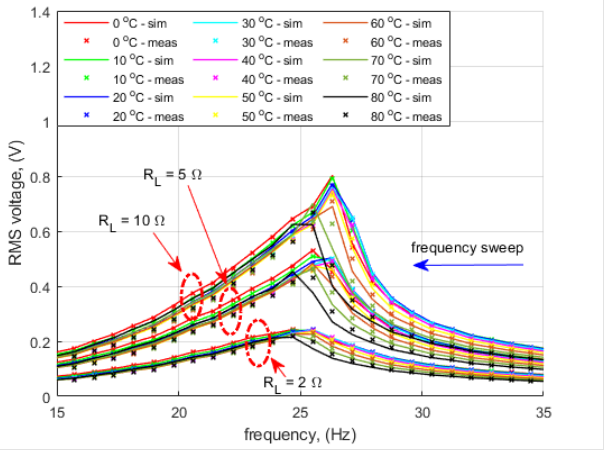

Fig.4. Measured and calculated frequency response characteristics of the RMS voltage for different temperatures and loads at an acceleration of 10 m/s² – vibration frequency decreasing from 35 to 15 Hz.

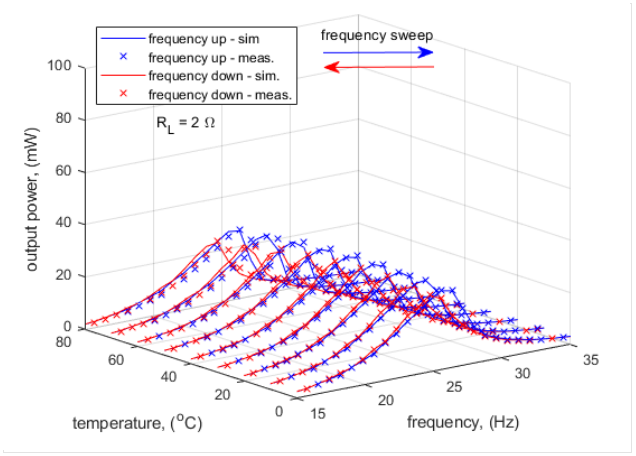

Fig.5. Measured and calculated frequency response characteristics of output power for different temperatures at a load of 2 Ω.

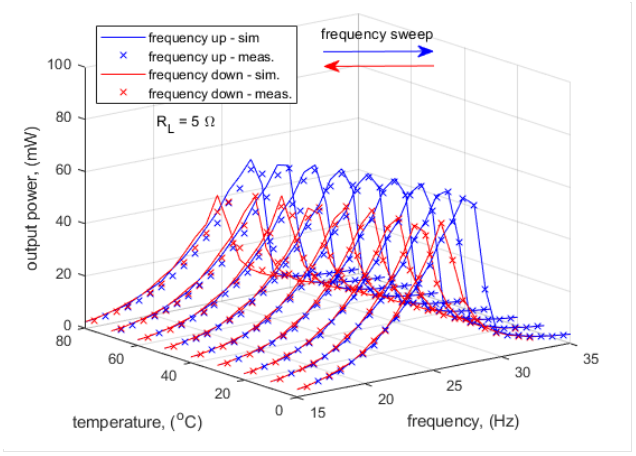

Fig.6. Measured and calculated frequency response characteristics of output power for different temperatures at a load of 5 Ω.

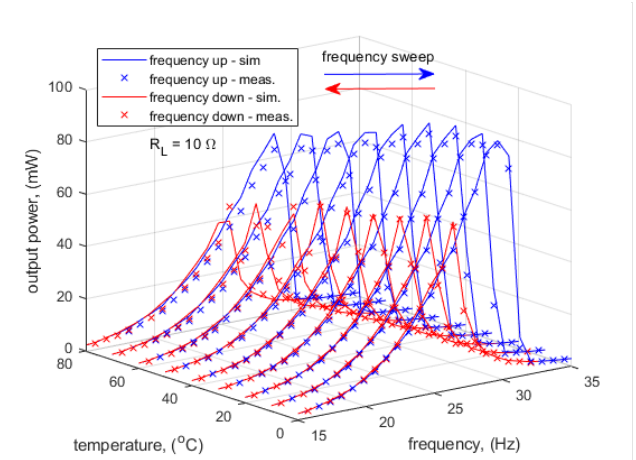

Fig.7. Measured and calculated frequency response characteristics of output power for different temperatures at a load of 10 Ω.

effect of temperature on the voltage values is similar to the previous case.

Figures 5, 6, and 7 also present the calculated and measured frequency response characteristics for three different loads, but they show the output power. The hysteresis phenomenon related to increasing and decreasing vibration frequencies can be observed. The maximum power is obtained at a temperature of 0°C and a load resistance of 10 Ω for a frequency of 29.6 Hz, with a value of 90.31 mW.

The presented results clearly show that the simulations conducted for the model obtained through optimization closely reflect the actual measurements. Despite minor deviations between the measurement results and simulations, particularly around the resonant frequency, the theoretical model can be effectively used to predict the voltage and output power of such devices under different temperature conditions. The temperature coefficients determined in this study are specific to the tested energy harvester configuration. Changes in the type of permanent magnets or beam material may affect these coefficients, requiring recalibration for each configuration to maintain accurate modeling.

4. DYNAMIC ANALYSIS FOR DIFFERENT TEMPERATURES

The identification of temperature coefficients enabled a series of simulations to illustrate the effect of ambient temperature on the parameters and dynamics of the studied vibration energy harvesting system. As shown in Figures 3–7, the highest voltage and power output are achieved with a load resistance of 10 Ω. Therefore, this resistance value was selected for further analysis, as maintaining a sufficient output voltage is essential in practical applications to ensure compatibility with an AC/DC converter. Figure 8 shows the computed values of the magnetic force and the derivative of the flux linkage with the coil as a function of temperature. As can be observed, an increase in temperature significantly reduces the absolute values of these parameters, which leads to a decrease in the output voltage of the harvesters.

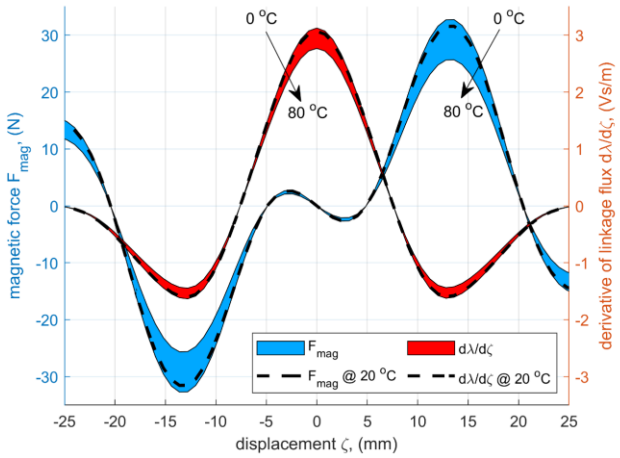

Fig.8. Computed magnetic force and derivative of flux linkage depending on yoke displacement and ambient temperature

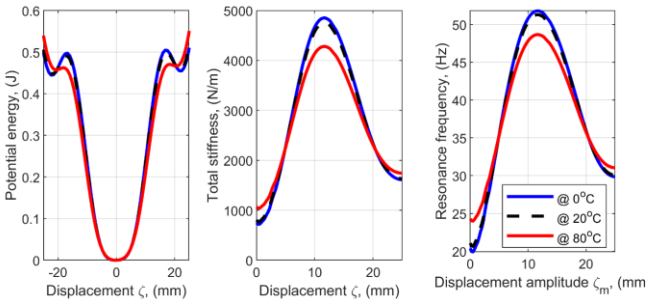

Fig.9. Computed potential energy, total stiffness and resonance frequency for different yoke displacement and ambient temperature

Figure 9 presents the computed potential energy, total stiffness (as the sum of the mechanical stiffness of the beam and the magnetic stiffness), and the resonant frequency as a function of yoke displacement and ambient temperature. As can be observed, with an increase in temperature, the values of these three parameters decrease. Lower potential energy values at higher temperatures result in greater displacements of the yokes with permanent magnets. The total stiffness and resonant frequency values are related by equation (5). The greater the difference between the stiffness at zero displacement and the stiffness at maximum deflection, the wider the frequency band in which relatively high voltage is generated. The considered system was designed for a displacement amplitude of 4 mm. The natural frequency of the beam is 20 Hz, while at the nominal displacement, the system's resonant frequency, due to the additional magnetic force, is 30 Hz. This results in a wide frequency band. As can be seen, an increase in temperature reduces the difference in total stiffness between the zero displacement point and, for example, a displacement of 4 mm. Consequently, the range of resonant frequencies also decreases, which is a disadvantage in this type of system.

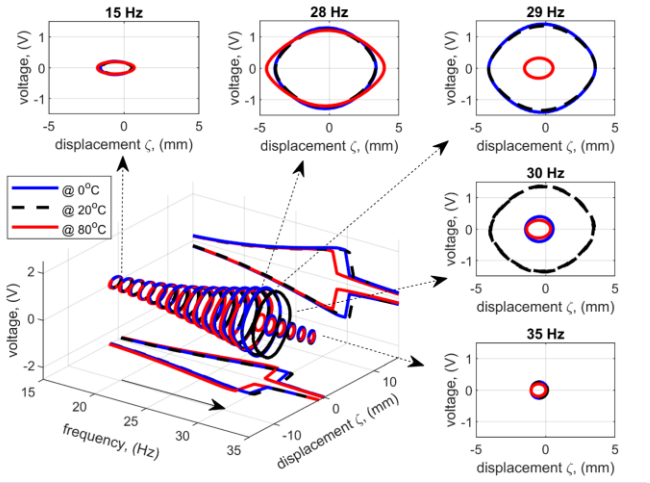

Fig.10. Trajectory of electromagnetic energy harvester for a_{RMS} = 10 m/s^2 and vibration frequency sweep from 15 to 35 Hz

Figures 10 and 11 compare the trajectories for increasing vibration frequencies (from 15 to 35 Hz) and decreasing frequencies (from 35 to 15 Hz). As can be observed, at 80°C,

the frequency band is reduced by about 2 Hz compared to the band at 0°C and 20°C. For the frequencies where resonance occurs at each ambient temperature (28 Hz in Fig. 10 and 26 Hz in Fig. 11), it is clearly visible that larger displacements are achieved at higher temperatures, which is related to lower potential energy (Fig. 9). However, despite the larger displacements, the voltage induced in the harvester's winding is lower compared to the voltage generated at lower temperatures. This is due to the negative effect of high temperature on the value of the flux linkage derivative (Fig. 8).

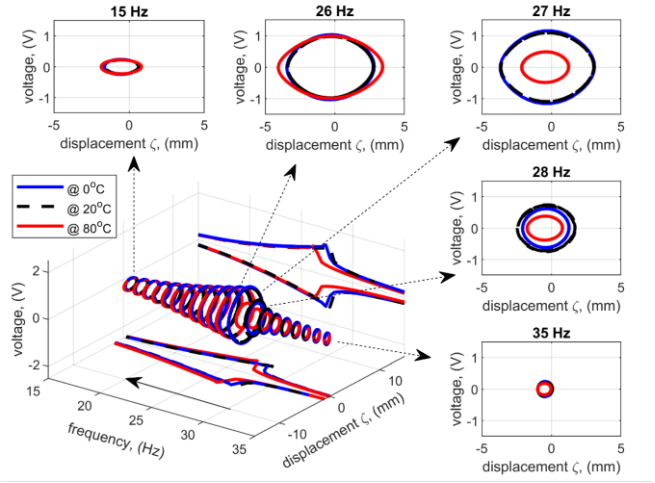

Fig.11. Trajectory of electromagnetic energy harvester for a_{RMS} = 10 m/s^2 and vibration frequency sweep from 35 to 15 Hz

5. CONCLUSIONS

The article analyzes the impact of temperature on the properties of a nonlinear electromagnetic vibration energy harvester, which can be used in autonomous power systems such as IoT devices. The research results showed that ambient temperature affects key device parameters, such as the stiffness of the beam, damping, and the magnetic properties of the magnets. An increase in temperature leads to a reduction in mechanical and magnetic stiffness, resulting in a decrease in the resonant frequency and output voltage. These phenomena also lead to a narrowing of the frequency band within which the device can effectively generate energy.

The proposed mathematical model, which incorporates temperature coefficients, was experimentally verified and demonstrated good agreement with the measurement results, particularly in the mid-range temperatures. Discrepancies at higher temperatures may be due to nonlinearities associated with magnetic interactions and imperfections in the model. Nevertheless, the developed model can successfully be used for optimizing the design of such harvesters in various environmental conditions.

The conducted research provides valuable insights into the dynamics of the system at different temperatures and may contribute to a better understanding of how to design more reliable energy harvesters capable of operating in varying environmental conditions.

[1] J.P. Norenberg, R. Luo, V.G. Lopes, J.V.L.L. Peterson, A. Cunha, "Nonlinear dynamics of asymmetric bistable energy harvesters," *Int J Mech Sci*, vol. 257, 2023. https://doi.org/10.1016/j.ijmecsci.2023.108542.

[2] F. Ali, W. Raza, X. Li, H. Gul, K.H. Kim, "Piezoelectric energy harvesters for biomedical applications," *Nano Energy* , vol. 57, pp. 879–902, 2019. https://doi.org/10.1016/J.NANOEN.2019.01.012.

[3] S.S. Won, M. Kawahara, S. Glinsek, J. Lee, Y. Kim, C.K. Jeong, A.I. Kingon, S.H. Kim, "Flexible vibrational energy harvesting devices using strain-engineered perovskite piezoelectric thin films," *Nano Energy*, vol. 55, pp. 82–192, 2019, https://doi.org/10.1016/J.NANOEN.2018.10.068.

[4] N. Shahraki, I. Jenab, W. Shen, "A Comprehensive Review on Energy Harvesting Integration in Internet of Things Applications," *Sensors*, vol. 21, no. 9, p. 3097, 2021, https://doi.org/10.3390/s21093097.

[5] M.A.A. Abdelkareem, L. Xu, M.K.A. Ali, A. Elagouz, J. Mi, S. Guo, Y. Liu, L. Zuo, "Vibration energy harvesting in automotive suspension system: A detailed review," *Appl Energy*, vol. 229, pp. 672–699, 2018, https://doi.org/10.1016/J.APENERGY.2018.08.030.

[6] J.D. Phillips, "Energy Harvesting in Nanosystems: Powering the Next Generation of the Internet of Things," *Frontiers in Nanotechnology*, vol. 3, 2021, https://doi.org/10.3389/FNANO.2021.633931.

[7] S. Kazemi, M. Nili-Ahmadabadi, M.R. Tavakoli, R. Tikani, "Energy harvesting from longitudinal and transverse motions of sea waves particles using a new waterproof piezoelectric waves energy harvester," *Renew Energy*, vol. 179, pp. 528–536, 2021, https://doi.org/10.1016/J.RENENE.2021.07.042.

[8] N. Sezer, M. Koç, "A comprehensive review on the state-of-the-art of piezoelectric energy harvesting," *Nano Energy*, vol. 80, 2021, https://doi.org/10.1016/J.NANOEN.2020.105567.

[9] S. Chalasani, J.M. Conrad, "A survey of energy harvesting sources for embedded systems," *Proceedings of IEEE Southeastcon*, Huntsville, Alabama, pp. 442–447, 2008, https://doi.org/10.1109/secon.2008.4494336.

[10] V.R. Challa, M.G. Prasad, Y. Shi, F.T. Fisher, "A vibration energy harvesting device with bidirectional resonance frequency tunability," *Smart Mater Struct*, vol. 17, 2008, https://doi.org/10.1088/0964-1726/17/01/015035.

[11] P.D. Mitcheson, E.M. Yeatman, G.K. Rao, A.S. Holmes, T.C. Green, "Energy harvesting from human and machine motion for wireless electronic devices," *Proceedings of the IEEE*, vol. 96, pp. 1457–1486, 2008, https://doi.org/10.1109/JPROC.2008.927494.

[12] M.F. Daqaq, R. Masana, A. Erturk, D.D. Quinn, "On the role of nonlinearities in vibratory energy harvesting: A critical review and discussion," *Appl Mech Rev*, vol. 66, 2014, https://doi.org/10.1115/1.4026278.

[13] M. Kulik, R. Gabor, M. Jagieła, "Surrogate Model for Design Uncertainty Estimation of Nonlinear Electromagnetic Vibration Energy Harvester," *Energies*, vol. 15, 2022, https://doi.org/10.3390/EN15228601.

[14] P.F. Pelz, P. Groche, M.E. Pfetsch, M. Schaeffner, eds., *Mastering Uncertainty in Mechanical Engineering*, Springer, 2021, https://doi.org/10.1007/978-3-030-78354-9.

[15] X.Q. Wang, Y. Liao, M.P. Mignolet, "Uncertainty Analysis of Piezoelectric Vibration Energy Harvesters Using a Finite Element Level-Based Maximum Entropy Approach," *ASCE-ASME Journal of Risk and Uncertainty in Engineering Systems, Part B: Mechanical Engineering*, vol. 7, 2021, https://doi.org/10.1115/1.4049208.

[16] H. Liang, G. Hao, O.Z. Olszewski, "A review on vibration-based piezoelectric energy harvesting from the aspect of compliant mechanisms," *Sens Actuators A Phys*, vol. 331, pp. 112743, 2021, https://doi.org/10.1016/J.SNA.2021.112743.

[17] K. Pancharoen, D. Zhu, S.P. Beeby, "Temperature dependence of a magnetically levitated electromagnetic vibration energy harvester," *Sens Actuators A Phys*, vol. 256, pp. 1–11, 2017, https://doi.org/10.1016/J.SNA.2017.01.011.

[18] E. Arroyo, Y. Jia, S. Du, S. -T. Chen, A.A. Seshia, "Experimental and Theoretical Study of a Piezoelectric Vibration Energy Harvester Under High Temperature," *Journal of Microelectromechanical Systems*, vol. 26, no. 6, pp. 1216-1225, 2017, https://doi.org/10.1109/JMEMS.2017.2723626.

[19] E. Blokhina, A. El Aroudi, E. Alarcon, D. Galayko, *Nonlinearity in Energy Harvesting Systems: Micro- and Nanoscale Applications*, Springer, 2016, https://doi.org/10.1007/978-3-319-20355-3.

[20] M. Kulik, M. Jagieła, M. Łukaniszyn, "Surrogacy-based maximization of output power of a low-voltage vibration energy harvesting device," *Applied Sciences*, vol. 10, 2020, https://doi.org/10.3390/APP10072484.

[21] G. Akoun, J.P. Yonnet, "3D analytical calculation of the forces exerted between two cuboidal magnets," *IEEE Trans Magn*, vol. 20, pp. 1962–1964, 1984, https://doi.org/10.1109/TMAG.1984.1063554.

[22] J. Eargle, *Electroacoustical reference data*, Springer, 1994.